Observations of bispectra of shoaling surface gravity waves

By STEVE ELGAR AND R. T. GUZA

J. Fluid Mech. (1985), *vol.* 161, *pp.* 425–448
Printed in Great Britain

Observations of bispectra of shoaling surface gravity waves

By STEVE ELGAR† AND R. T. GUZA

Scripps Institution of Oceanography, Mail Code A-022, University of California, La Jolla, California 92093

(Received 15 April 1985)

Aspects of the nonlinear dynamics of waves shoaling between 9 and 1 m water depths are elucidated via the bispectrum. Bispectral-signal levels are generally high, indicating significant nonlinear coupling. In 9 m depth, the biphases of interactions involving frequencies at, and higher than, the peak of the energy spectra are suggestive of Stokes-like nonlinearities (Hasselman, Munk & MacDonald 1963). Further shoaling gradually modifies these biphases to values consistent with a wave profile that is pitched shoreward, relative to a vertical axis. Bicoherence and biphase observations with a double-peaked (swell and wind-wave) power spectrum provide evidence for excitation of modes at intermediate frequencies via difference interactions, as well as the sum interactions responsible for harmonic growth. Shoreward-propagating low-frequency (surf-beat) energy is shown to have statistically significant coupling to higher-frequency modes within the power-spectral peak. In 18 m depth, the biphase of these interactions is close to 180°, a value consistent with the classical concept of bound long waves. In shallower water, however, substantial biphase evolution occurs, and there is no longer a unique phase relationship between surf beat and the envelope of high-frequency waves. The contributions to sea-surface-elevation skewness and asymmetry (with respect to a vertical axis) from interactions among various wave triads are given by the real and imaginary parts of the bispectrum, respectively. In very shallow water, coupling between surf beat and higher-frequency waves results in a skewness with sign opposite to, and about 40% of the magnitude of, the skewness resulting from interactions between the power-spectral-peak frequency and higher frequencies.

1. Introduction

Since its introduction more than twenty years ago (Hasselman, Munk & MacDonald 1963), bispectral analysis has been utilized by many investigators to study nonlinear phenomena. Hasselman *et al.* (1963) obtained good agreement between observations of bispectra of ocean-surface gravity waves in intermediate water depth (11 m) and predictions based on Stokes-like, non-resonant, nonlinear interactions. Nonlinearities in a wide range of other phenomena have been studied (with varying degrees of success) with bispectral techniques since the seminal paper of Hasselman *et al.* (1963), for example, economic time series (Godfrey 1965), brain-wave emissions (Barnett *et al.* 1971; Huber *et al.* 1971), and machinery vibrations (Sato, Sasaki & Taketani 1980, and references therein). Van Atta and coworkers (e.g. Yeh & Van Atta 1973;

† Present address. Engineering Science Department, College of Engineering, University of Idaho, Moscow, Idaho 83843, USA.

Lii, Rosenblatt & Van Atta 1976; Helland, Van Atta & Stegun 1977; Van Atta 1979) have investigated the nonlinear transfer of energy in turbulent flows using bispectral methods. Nonlinear interactions between modes of density fluctuations in plasmas have been studied with bispectral techniques by Kim & Powers (1978, 1979) and Kim *et al.* (1980).

Simultaneous with these data-analysis applications, the mathematical and statistical properties of the bispectrum have been developed. Brillinger (1965), Rosenblatt & Van Ness (1965), and Brillinger & Rosenblatt (1966*a*, *b*) give some of the statistical properties of higher-order spectra. Haubrich (1965) and Hinnich & Clay (1968), as well as Kim & Powers (1979), discuss the statistics of bicoherence.

The present study returns to the question of ocean gravity waves, but considers waves in water depths between 9 m and 1 m. Waves in this shoaling region are particularly well suited to analysis with bispectral techniques for several reasons, the most important being that bispectral-signal levels are relatively high. The statistical variability of bispectra is such that many degrees of freedom (relative to one-dimensional spectra) are required for statistical stability, with the required degrees of freedom generally increasing with decreased strength of the bispectral signal. This constraint has led McComas & Briscoe (1980) to conclude that bispectral analysis of interactions between certain internal wave frequencies would be fruitless. On the other hand, waves in the shoaling region are of short enough timescale that many degrees of freedom can be obtained without losing stationarity. This combination of many degrees of freedom and high bispectral-signal levels leads to statistical stability of the bispectral estimates in the present study.

Preliminary definitions and properties of bispectra are reviewed in §2, and the field experiment is described in §3. Observations of bispectra for several different shoaling-wave power spectra are discussed in detail in §4, where phenomena undetectable with one-dimensional spectral analysis are presented. Data with broad-band power spectra show some surprising similarities to narrow-band data in certain aspects of bispectral evolution (§4.1), in particular the biphase. Similarities are also evident in the evolution of sea-surface-elevation skewness and asymmetry (about a vertical axis). The contributions to the skewness and asymmetry from different wave triads are examined with the bispectrum. Evidence of excitation of modes via difference interactions as well as sum interactions is observed in a data set with a double-peaked power spectrum. Low-frequency motions (surf beat) are shown to be nonlinearly coupled to energy at frequencies closely spaced within the power-spectral peak (§4.2), as suggested by the classical notion of surf beat (Munk 1949). However, biphase analysis shows that the surf-beat modes in the shoaling region are not 180° out of phase with the envelope of higher-frequency waves. Cross-bispectra are used to show that surf-beat motions on the beach face (swash) are nonlinearly coupled to higher-frequency modes seaward of the surf zone (§4.3).

2. Definitions and properties of the bispectrum

Let a stationary random process be represented as

$$\eta(x,t) = \sum_{n=1}^{N} A_n \mathrm{e}^{\mathrm{i}(k_n x - \omega_n t)} + A_n^* \mathrm{e}^{-\mathrm{i}(k_n x - \omega_n t)}, \tag{2.1}$$

where k is the wavenumber given by the dispersion relationship, ω is the radian frequency, the subscript n is a frequency (modal) index, an asterisk indicates complex conjugation, and the A_n are complex Fourier coefficients. The auto-bispectrum is

formally defined as the Fourier transform of the third-order correlation function of the time series (Hasselman *et al.* 1963)

$$B(\omega_1,\omega_2)=\left(\frac{1}{2\pi}\right)^2\int_{-\infty}^{\infty}\int_{-\infty}^{\infty}S(\tau_1,\tau_2)\,\mathrm{e}^{-\mathrm{i}\omega_1\tau_1-\mathrm{i}\omega_2\tau_2}\,\mathrm{d}\tau_1\,\mathrm{d}\tau_2, \tag{2.2}$$

where

$$S(\tau_1,\tau_2)=\mathrm{E}[\eta(t)\,\eta(t+\tau_1)\,\eta(t+\tau_2)] \tag{2.3}$$

with E[ ] the expected value, or average, operator. The digital bispectrum, appropriate for discretely sampled data, is (Haubrich 1965; or see Kim & Powers 1979 for a complete derivation)

$$B(\omega_k,\omega_j)=\mathrm{E}[A_{\omega_k}A_{\omega_j}A^*_{\omega_k+\omega_j}]. \tag{2.4}$$

Similarly, the power spectrum is defined here as

$$P(\omega_k)=\tfrac{1}{2}\mathrm{E}[A_{\omega_k}A^*_{\omega_k}]. \tag{2.5}$$

From (2.4) the bispectrum is zero if the average triple product of Fourier coefficients is zero. This occurs if the modes are independent of each other, i.e. for the random phase relationships between Fourier modes in a linear wave field. Using symmetry properties, the bispectrum can be uniquely described by its values in a bi-frequency octant. For a digital time series with Nyquist frequency ω_N, the bispectrum is uniquely defined within a triangle in (ω_1,ω_2)-space with vertices at $(\omega_1=0,\omega_2=0)$, $(\omega_1=\omega_{N/2},\omega_2=\omega_{N/2})$, and $(\omega_1=\omega_N,\omega_2=0)$.

The well-known result that the mean cube of the time series is related to the real part of the bispectrum is obtained by forming $\mathrm{E}[\eta(t)^3]$ from the expected value of the cube of the right-hand side of (2.1.):

$$\mathrm{E}[\eta(t)^3]=12\sum_n\sum_l\mathrm{Re}\{B(\omega_n,\omega_l)\}+6\sum_n\mathrm{Re}\{B(\omega_n,\omega_n)\}, \tag{2.6}$$

where $n>l$ and Re { } signifies the real part. The skewness is obtained from (2.6) by normalizing by $E[\eta(t)^2]^{\frac{3}{2}}$. A quantity analogous to skewness, hereinafter called the asymmetry, is defined here as

$$\text{Asymmetry}=\left[12\sum_n\sum_l\mathrm{Im}\{B(\omega_n,\omega_l)\}+6\sum_n\mathrm{Im}\{B(\omega_n,\omega_n)\}\right]\Big/\mathrm{E}[\eta^2]^{\frac{3}{2}}, \tag{2.7}$$

where $n>l$ and Im { } signifies the imaginary part. It can be shown that the asymmetry is the skewness of the Hilbert transform of the time series, and is also related to the skewness of the slopes of the time series,

$$\mathrm{E}\left[\left(\frac{\partial\eta}{\partial t}\right)^3\right]=12\sum_n\sum_l\omega_n\,\omega_l\,\omega_{n+l}\,\mathrm{Im}\{B(\omega_n,\omega_l)\}$$
$$+6\sum_n\omega_n\,\omega_n\,\omega_{2n}\,\mathrm{Im}\{B(\omega_n,\omega_n)\}+\text{terms of order }\frac{\partial A}{\partial t}, \tag{2.8}$$

where $n>l$. The expression for $\mathrm{E}[(\partial\eta/\partial x)^3]$ is the same as (2.8) with ω_i replaced by k_i.

It is convenient to recast the bispectrum into its normalized magnitude and phase, called the bicoherence and biphase, given respectively by (Kim & Powers 1979)

$$b^2(\omega_1,\omega_2)=\frac{|B(\omega_1,\omega_2)|^2}{\mathrm{E}[|A_{\omega_1}A_{\omega_2}|^2]\,\mathrm{E}[|A_{\omega_1+\omega_2}|^2]}, \tag{2.9}$$

$$\beta(\omega_1,\omega_2)=\arctan\left[\frac{\mathrm{Im}\{B(\omega_1,\omega_2)\}}{\mathrm{Re}\{B(\omega_1,\omega_2)\}}\right]. \tag{2.10}$$

Writing the Fourier coefficients as a magnitude and phase,

$$A_n = |A_n| e^{-i\theta_n}, \tag{2.11}$$

the biphase is (Kim *et al.* 1980)

$$\beta(\omega_i, \omega_j) = \theta_{\omega i} + \theta_{\omega_j} - \theta_{\omega i + \omega_j}. \tag{2.12}$$

For this bicoherence normalization (2.9), $0 \leqslant b \leqslant 1$. Various other combinations of the A_n have been used to normalize the bicoherence. If, however, the denominator of (2.9) is replaced with (Haubrich 1965; and others) $\mathrm{E}[|A_{\omega_1}|^2]\,\mathrm{E}[|A_{\omega_2}|^2]\,\mathrm{E}[|A_{\omega_1+\omega_2}|^2]$, it is no longer true that $b \leqslant 1$. For the data considered in the present study, such a normalization led to values of $b > 2.5$.

For a finite-length time series even a truly Gaussian process will have a non-zero bispectrum. A 95% significance level on zero bicoherence is given by Haubrich (1965) as

$$b^2_{95\%} \geqslant 6/\text{d.o.f.} \tag{2.13}$$

where d.o.f. is the number of degrees of freedom. Preliminary numerical simulations similar to Haubrich (1965) indicate that the 95% significance levels for the normalization given in (2.9) are about $\frac{1}{4}$ the value given by (2.13), which yields a value closer to the 99% significance level for bicoherences calculated with (2.9). Equation (2.13) is used below, and is a conservative estimate of 95% significance levels. The precise values of bicoherence significance levels are not important here. Confidence limits on the estimates of bicoherence depend on the true value of the bicoherence, but it has been shown that the variance of bicoherence estimates is less than 2/d.o.f. (Hinich & Clay 1968; Kim & Powers 1979). Confidence levels for estimates of biphase depend on bicoherence values and the number of degrees of freedom. Biphase estimates for frequency pairs with very low bicoherence are unstable, and tend to be randomly distributed between $-\pi$ and π, while for frequency pairs with high bicoherence levels the estimates of biphase are stable. Analogous to phase estimates from standard cross-spectra (e.g. Jenkins & Watts 1968, figure 9-3), the stability of biphase estimates at fixed bicoherence must increase with increasing number of degrees of freedom. However, quantitative estimates of biphase confidence levels are not available. Although some of the data analysed below have only moderate (but statistically significant) bicoherence values, the biphases are quite stable, apparently owing to the large number of degrees of freedom (typically 150–300).

For a 3-wave system, Kim & Powers (1979) show that $b^2(\omega_i, \omega_j)$ represents the fraction of power at frequency $\omega_i + \omega_j$ due to quadratic coupling of the 3 modes (ω_i, ω_j, and $\omega_i + \omega_j$). No such simple interpretation for the bicoherence is possible in a broad-band process where a particular mode may be simultaneously involved in many interactions (McComas & Briscoe 1980). Nevertheless, the bicoherence does give an indication of the relative degree of phase coupling between triads of waves, with $b = 0$ for random phase relationships, and $b = 1$ for a maximum amount of coupling. Work in progress concerns the statistical properties (e.g. biphase confidence limits) and physical significance of bispectral quantities in broad-band processes.

3. Experiment and data reduction

Most of the field data discussed were obtained at Santa Barbara, California, during the Nearshore Sediment Transport Study experiment conducted in January and February 1980 (Gable 1981). The observations used in the present study were

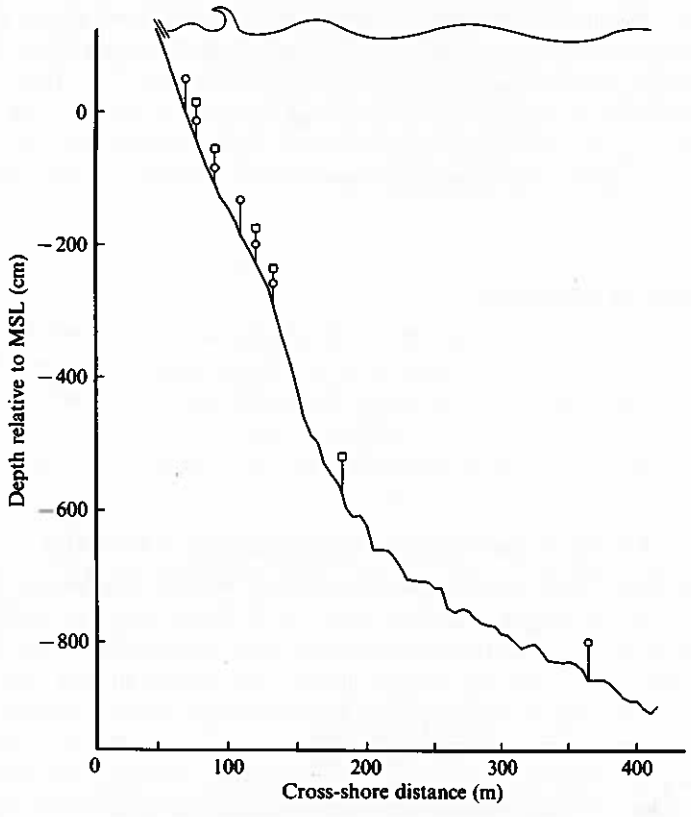

FIGURE 1. Measured beach profile and instrument locations along a line perpendicular to the beach. Circles are pressure gauges, squares are bi-directional current meters, and a runup meter lies on the beach face.

obtained primarily from near-bottom-mounted pressure sensors, located along a line perpendicular to the beach, from approximately 9 m depth to less than 1 m depth (300 m horizontal distance). Marsh McBirney electromagnetic current meters and a runup meter on the beach face were also used. A typical beach profile and sensor locations are shown in figure 1.

The gauges were sampled at 2 Hz for up to 5 h daily. Bulk statistics (variance, frequency of the spectral peak, etc.) and certain wave-group statistics (Elgar, Guza & Seymour 1984) were checked for stationarity. Data sets with any indication of nonstationarity were rejected. The selected data were processed by breaking the entire record into consecutive sections of 512 s each, resulting in a frequency resolution for the raw data of 0.00195 Hz. Bottom pressures measured in depths less than 6 m were converted to sea-surface elevation using finite-depth linear theory. Measurements in deeper water were not corrected for depth attenuation because the correction unrealistically amplifies small noise levels near the high-frequency cutoff ($f = 0.4$ Hz). Owing to the normalization in (2.9) and (2.10), and the fact that the depth-correction coefficients do not vary significantly within the frequency bands used here, there is negligible difference between the bicoherence and biphase of bottom pressure and sea-surface elevation. Statistical stability of bispectral estimates is gained by averaging bispectral values over 5×5 squares (or triangles along the diagonals) (except the 12 February data, figure 11, where 10×10 squares are used)

in (f_1, f_2)-space, where $f = 2\pi\omega$, and ensemble-averaging over many 512 s records. Similarly, power-spectral estimates are smoothed by merging 5 frequency bands and ensemble averaging over the collection of 512 s records. The final spectral and bispectral resolution is 0.0098 Hz (except 12 February, where the resolution is 0.0195 Hz). The number of degrees of freedom in the bispectra discussed here ranged from 160 to 310, mainly reflecting differences in the number of 512 s pieces available for averaging.

4. Observations of bispectra

This section describes the bispectra of shoaling waves observed in the field. The three data sets that will be discussed in detail have approximately the same total variance, but very different power spectra. First, interactions involving the swell and wind-wave bands ($0.04 < f < 0.4$ Hz) will be discussed, and then interactions involving the infragravity wave, or low-frequency band ($f < 0.04$ Hz), will be examined.

4.1. *Swell and wind-wave frequencies* ($f > 0.04$ Hz)

The 2 February wave field is dominated by swell ($f \sim 0.06$ Hz) from a distant storm. The significant wave height (defined here as 4 times the sea-surface standard deviation) in 4 m depth is 65 cm, and there is a very small peak at the first harmonic ($f = 0.12$ Hz, figure 2*a*). As the waves shoal, the power in the first and higher-harmonic ($f \sim 0.18$, 0.24, 0.30 Hz) peaks increases (figures 2*b–f*, upper panels). The growth of these harmonics is not predicted by any linear theory, but is well modelled by the nonlinear Boussinesq-type equations described in Freilich & Guza (1984) (see also figure 3 of Elgar & Guza 1985*a*). The bicoherence spectrum at the deepest sensor (figure 2*a*) indicates nonlinear coupling between modes within the power-spectral peak and modes at twice the peak's frequency. The convention is that the interactions involve f_1, f_2, and f_3, where $f_3 = f_1 + f_2$. For example, $b(0.06, 0.06) = 0.30$, indicating a self–self wave interaction at $f = 0.06$ Hz coupled to energy at $f = 0.12$ Hz. As the waves shoal, the excitation of phase-coupled harmonics is vividly reflected in the bicoherence. In 4 m depth (figure 2*c*), the bicoherence indicates stronger (than in deeper water) coupling within the peak ($b(0.06, 0.06) = 0.49$), and also coupling between the peak and its first two harmonics ($b(0.06, 0.12) = 0.28$; $b(0.06, 0.18) = 0.14$). In shallower water nonlinear coupling spreads not only to encompass interactions between the power-spectral peak and its higher harmonics, but also to interactions between the harmonics themselves. For example, in 2 m depth (figure 2*e*) $b(0.06, 0.24) = 0.16$; $b(0.12, 0.12) = 0.43$; $b(0.12, 0.18) = 0.41$; $b(0.18, 0.18) = 0.33$. Although these bispectral calculations indicate only that nonlinear coupling is occurring, and not the direction of energy flow (i.e. which modes are receiving energy), the sequence of energy spectra in figure 2 shows that energy is being received by high frequencies.

Along with the increase in bicoherence shown in figure 2, there is substantial biphase evolution as the waves shoal (figures 3 and 4). As mentioned in §3, for frequency pairs with very low values of bicoherence, the biphase is undefined, and can take on any value between $-\pi$ and π. In order to visualize the biphase values in the wind-wave frequency band, it is convenient to view the 3-dimensional perspective plots from a different angle than the bicoherence plots. Thus, figures 3, 7, and 11 are rotated, enabling a view of the wind-wave band frequency pairs that is unobstructed by the wall of low-frequency biphase noise. The evolution of biphases

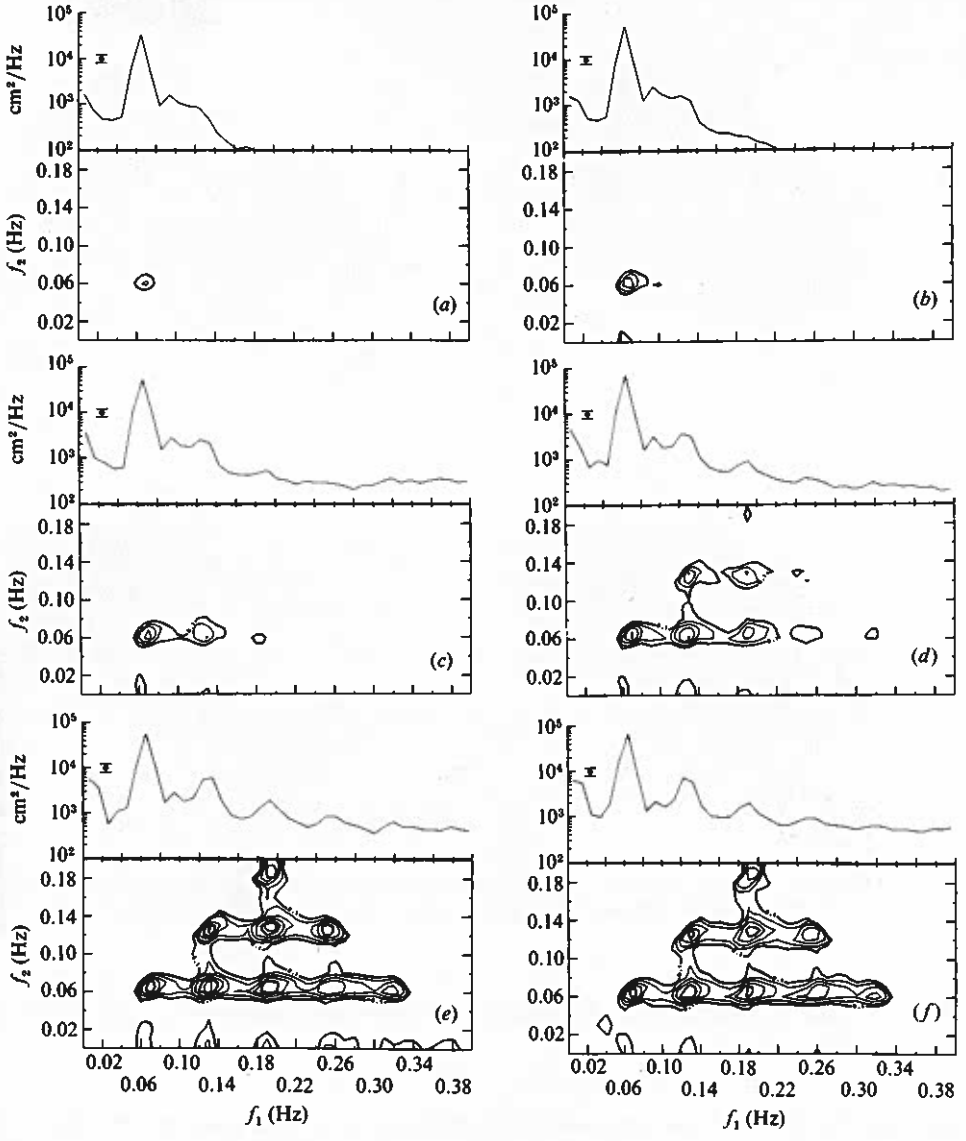

FIGURE 2. Power spectra and contours of bicoherence for the 2 February data at various depths. The power spectra (bars indicate 95% confidence levels) are immediately above the corresponding bicoherence plots. The minimum bicohrence-contour level is $b = 0.1$, with additional contours every 0.05. There are 310 degrees of freedom (d.o.f.) and the 95% significance level (according to (2.13)) for zero bicoherence is $b = 0.14$. Depths are (*a*) $h = 9.0$ m, (*b*) 6.4 m, (*c*) 3.9 m, (*d*) 2.7 m, (*e*) 2.0 m, (*f*) 1.3 m.

for a few selected frequency pairs (those pairs with the highest observed values of bicoherence, combinations of the power-spectral peak and its harmonics) are displayed in figure 4.

Features of the self–self interaction at the spectral peak in the 9 m depth data are consistent with Stokes-type nonlinearities. If the Stokes wave is represented as

$$\eta(x,t) = C_1 \cos\theta + C_2 \cos 2\theta + C_3 \cos 3\theta + \ldots, \tag{4.1}$$

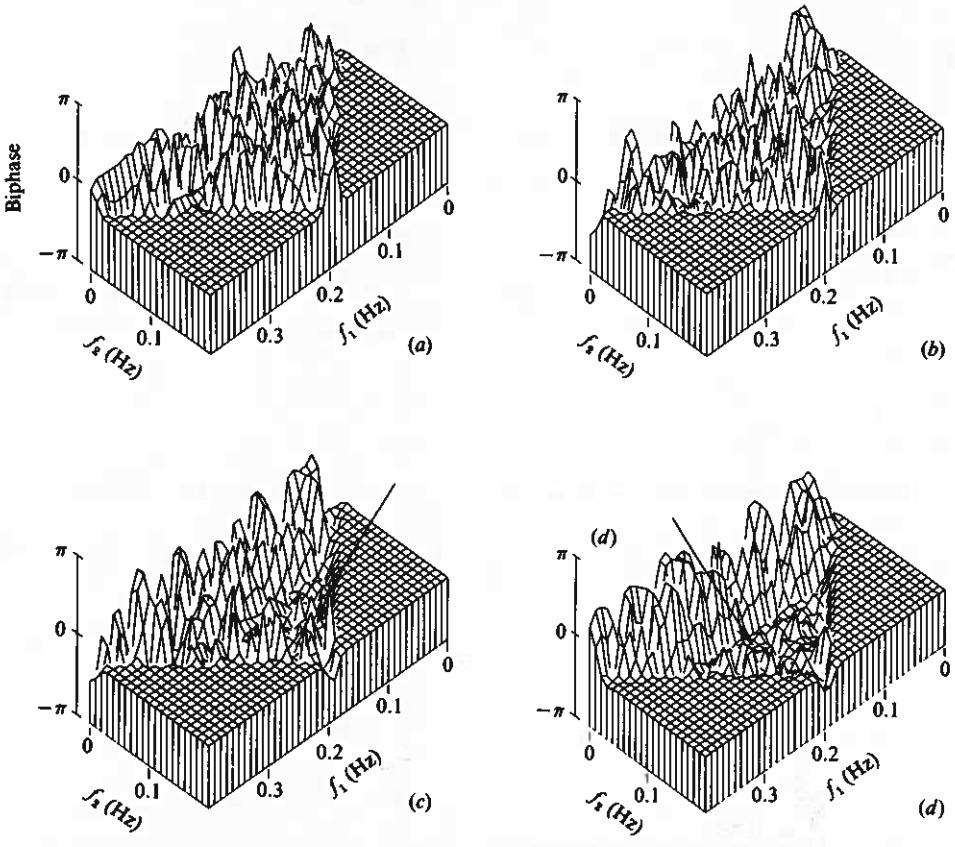

FIGURE 3. Biphase for the 2 February data set. The arrows indicate the plateau of approximately equal values of biphase. (*a*) $h = 9.0$ m, (*b*) 3.9 m, (*c*) 2.7 m, (*d*) 2.0 m.

where the C_i are functions of the amplitude, wavenumber and depth, and $\theta = kx - \omega t$, then the bispectrum is

$$B_{\text{Stokes}}(\omega_i, \omega_j) = [C_i C_j C_{i+j}, 0], \tag{4.2}$$

where $[\mathscr{R}, \mathscr{I}]$ denotes the real and imaginary parts of the bispectrum. Thus, for all harmonic frequencies the bicoherence is 1 and the biphase is zero. Directional spreading in the primary frequency band decreases the bicoherence (Hasselman *et al.* 1963), as does the presence of uncoupled waves at harmonic frequencies. As shown in figure 4, in 9 m depth, the two lowest-order interactions $[(f_p, f_p), (f_p, 2f_p)]$, where f_p is the frequency of the power-spectral peak, have biphase of about $-15°$, and two of the other interactions are also within 25° of the Stokes biphase ($\beta = 0°$). Since only the lowest-order interactions have significant bicoherence and substantial biphase stability, the 9 m data are interpreted as qualitatively consistent with Stokes-like nonlinearities. A similar conclusion, based on an analysis which included directional effects in 11 m depth, was reached by Hasselman *et al.* (1963).

As the waves shoal, the biphases of harmonic interactions tend towards $\beta = -\frac{1}{2}\pi$ (figure 4). The biphase perspective plots (figure 3) show that many frequencies, not just the harmonics (figure 4) are nonlinearly coupled, and have biphase values that approach $\beta = -\frac{1}{2}\pi$. In 4 m depth the harmonic-frequency pairs have similar

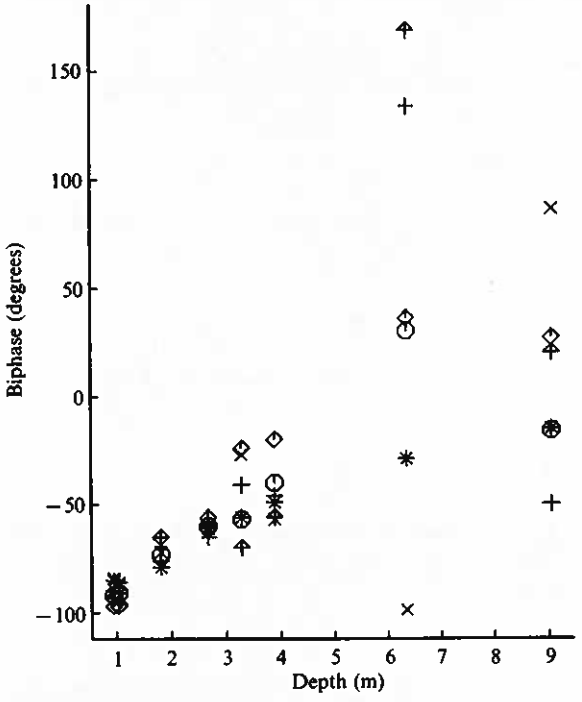

FIGURE 4. Biphase *versus* depth for selected frequency pairs for the 2 February data set. ✱ (f, f); ⊙, $(f, 2f)$; +, $(f, 3f)$; ×, $(f, 4f)$; ♠, $(2f, 2f)$; ◇, $(2f, 3f)$, where $f = 0.06$ Hz corresponds to the power-spectral-peak frequency.

values of biphase ($\beta \approx -50°$, figure 4). As the water depth decreases, the region of approximately constant biphase increases to encompass more and more frequency pairs, as shown by the increasing area of the plateau of approximately equal biphase values in figure 3. The values of almost all biphases steadily approaches $\beta = -\frac{1}{2}\pi$.

Since the biphase depends on the ratio of imaginary to real parts of the bispectrum, which are related to skewness and asymmetry, respectively, it is not surprising that the biphase is related to the wave's shape. Masuda & Kuo (1981) showed that a primary and its first harmonic with zero biphase is associated with a wave with sharp peaks and broad, flat troughs, but with symmetry about a vertical axis, as in a Stokes wave. On the other hand, a biphase of $-\frac{1}{2}\pi$ is associated with a wave pitched forward (i.e. vertical asymmetry), but symmetrical with respect to a horizontal axis (zero skewness). The observed evolution of biphase values is consistent with the visual observation that as waves shoal they evolve from a slightly peaked, nearly sinusoidal shape in deep water to a shape characterized by a steep forward face and a relatively gently sloping rear face (figure 5). In very shallow water (figure 5*e*, for example) the data are suggestive of a sawtooth shape. It is readily shown that the bispectrum of a sawtooth is

$$B_{\text{sawtooth}}(i,j) = \left[0, \frac{-8}{\pi^3(i^2j + ij^2)}\right], \tag{4.3}$$

so the sawtooth biphase is $\beta(i,j) = -\frac{1}{2}\pi$.

In contrast to the 2 February data, the 15 February data (figures 6 and 7) have quite broad-band energy spectra. The significant wave height in 4 m depth for the 15 February data is 65 cm, the same as the 2 February data. The 15 February energy

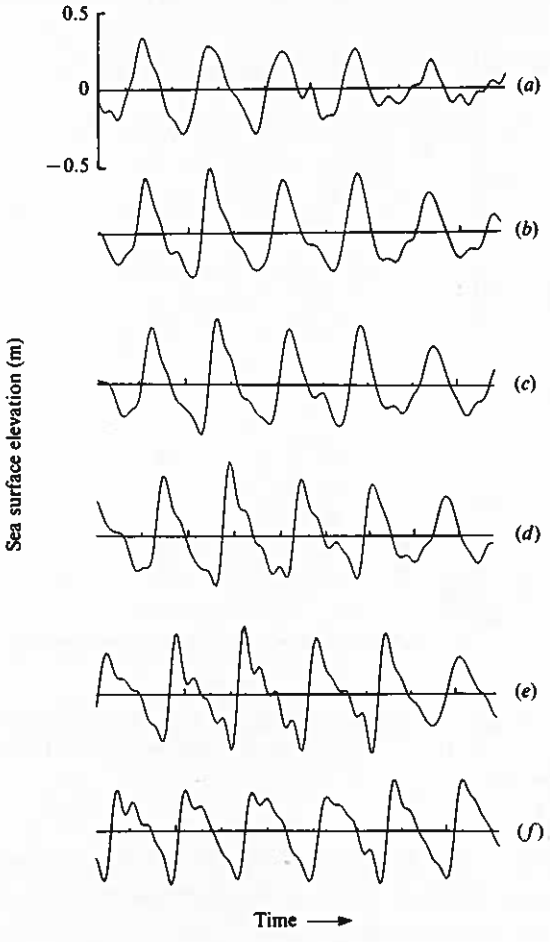

FIGURE 5. Sea-surface elevation *versus* time for a short section (about 90 s) of the 2 February data set. (*a*) $h = 8.7$ m, (*b*) 3.6 m, (*c*) 2.9 m, (*d*) 2.4 m, (*e*) 1.7 m, (*f*) 1.0 m.

spectra show very little evolution as the wave field shoals (figure 6, upper panels). The increase in high-frequency energy ($f > 0.2$ Hz) at the 4 m depth (figure 6*c*) is an artifact of not correcting the two deeper measurements (figure 6*a* and *b*) for depth attenuation. The bicoherences (figure 6) also show little structural evolution, although the average level of bicoherence does steadily increase from near zero in 9 m depth (figure 6*a*) to about $b = 0.15$ in 0.9 m depth (figure 6*f*). Even though this value of bicoherence is not large, it indicates that significant nonlinear coupling is occurring. In contrast to the sharp peaks and steep valleys of the bicoherence spectra for the narrow-band 2 February data (figure 2), the 15 February data evolve from near-zero bicoherence values to low (but non-zero) values broadly spread over most of the wind-wave frequency band pairs (figure 6).

Despite the radically different evolution of power spectra and bicoherence for the 2 February (figure 2) and 15 February (figure 6) data sets, the evolution of biphase is remarkably similar (compare figures 3 and 7). The 15 February data have no statistically significant equivalent of the Stokes-like interaction within the narrow spectral peak of the 2 February data in 9 m depth, but by the shallower sensors (figures 7*c* and *d*) no features distinguish the biphase spectra of the broad-band data

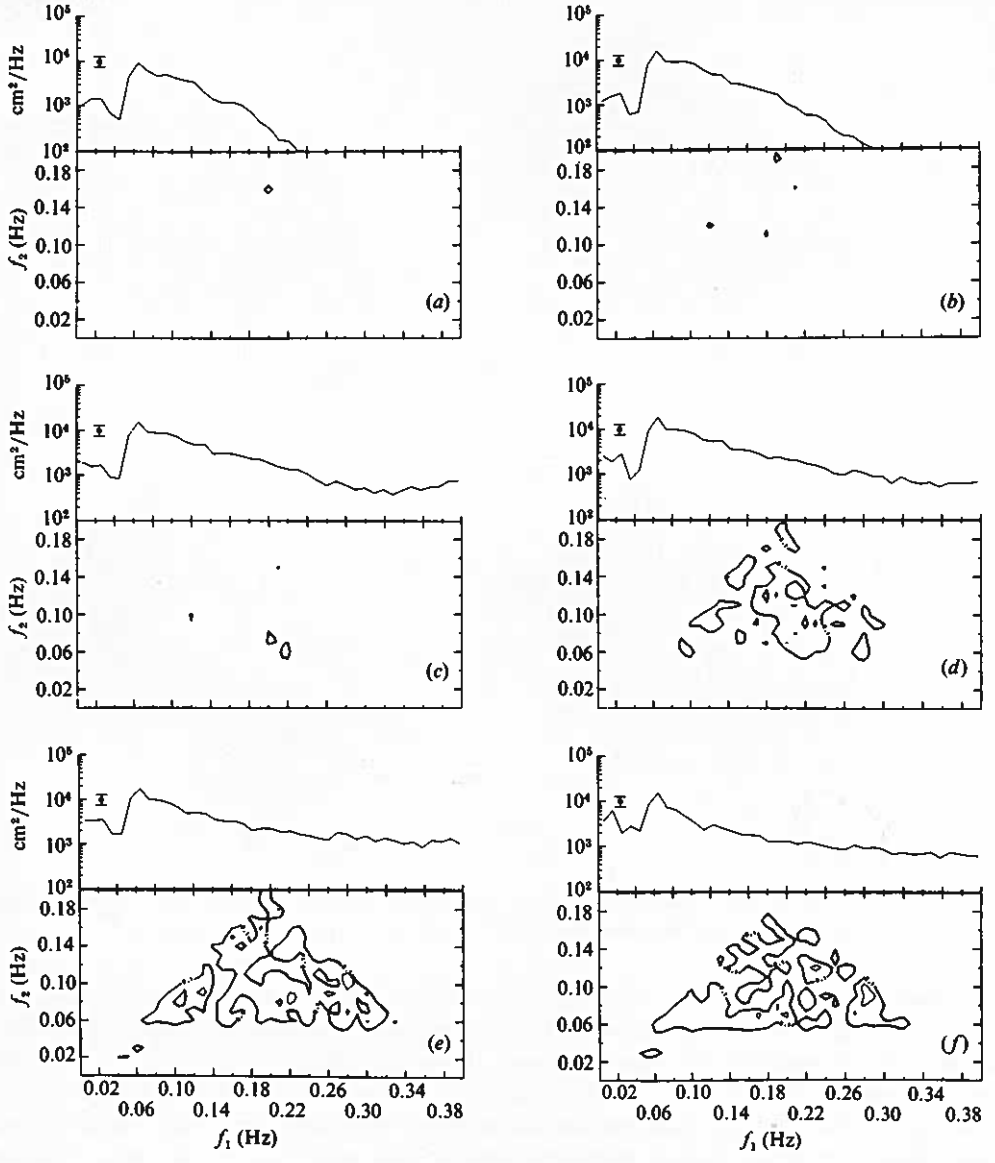

FIGURE 6. Power spectra and contours of bicoherence for the 15 February data set, with the same format as figure 2: d.o.f. = 160, and the 95 % significance level ((2.13)) for zero bicoherence is $b = 0.19$. Depths are (*a*) $h = 8.7$ m, (*b*) 6.0 m, (*c*) 3.5 m, (*d*) 2.2 m, (*e*) 1.6 m, (*f*) 0.9 m.

(figure 7) from the narrow-band data (figure 3). The similar biphases are not surprising considering that the shapes of waves in very shallow water are qualitatively similar for broad and narrow power spectra, i.e. steep front faces and flat rear slopes (figures 5 and 8).

Although the bicoherence spectra for the 2 February and 15 February data sets are quite different in structure, various integrals of the bispectrum of each data set are similar. In particular, the skewness (2.6) and asymmetry (2.7) of each data set (band-pass filtered between $f = 0.04$ and $f = 0.4$ Hz) have similar evolution and values, as shown in figure 9. The skewness is relatively low in 9 m depth, increases

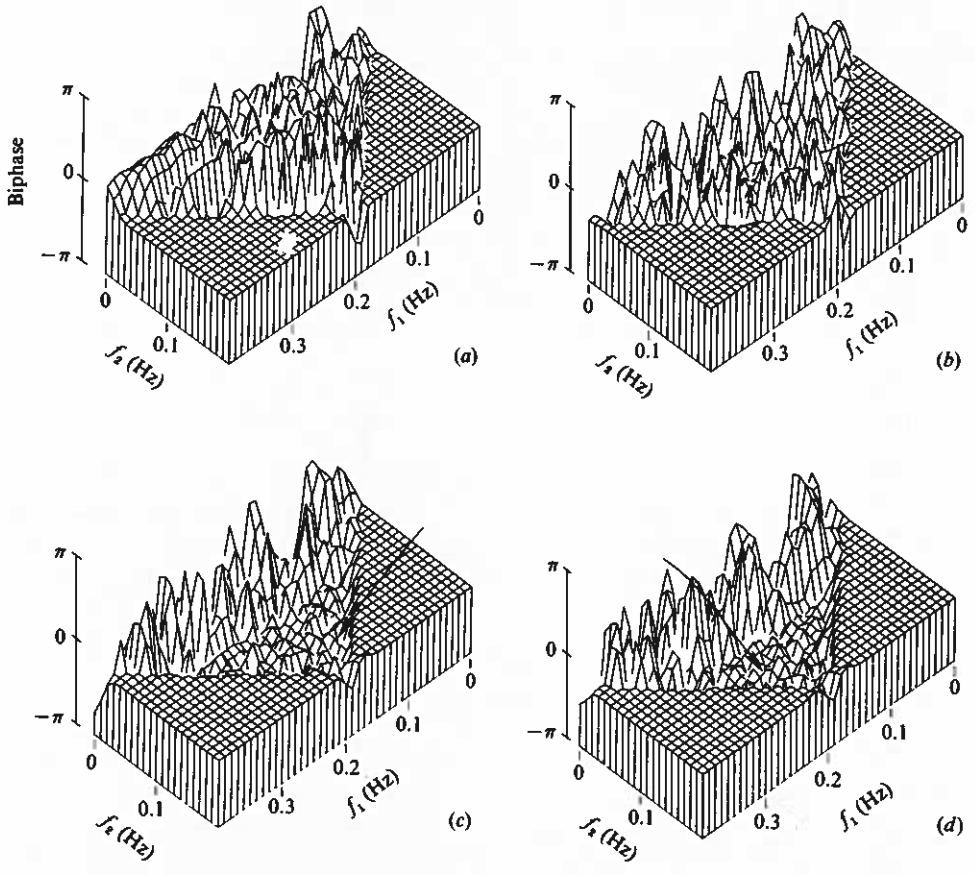

FIGURE 7. Biphase for the 15 February data set. The arrows indicate the plateau of approximately equal values of biphase. (*a*) $h = 8.7$ m, (*b*) 3.5 m, (*c*) 2.2 m, (*d*) 1.6 m.

to a maximum in about 2 m depth, and then decreases to near zero in even shallower water. The asymmetry has a near-zero value in 9 m, but increases (in absolute value, asymmetry is negative for shoaling waves in the coordinate frame used here) as the waves shoal, reaching a maximum value slightly shoreward of the skewness maximum. Similar structure of the skewness and asymmetry evolution was observed in several other data sets, with various power-spectral shapes, and with a wide range of wave heights. The slight decrease in asymmetry (figure 9) in very shallow water occurs at depths where substantial dissipation (wave breaking, loosely defined here as occurring at the depth where the linear energy flux is less than 85% of the energy flux measured in 4 m depth) begins to occur (depth = 1.0 m and 1.5 m for 2 February and 15 February, respectively).

The contributions to skewness and asymmetry from each frequency pair (i.e. the real and imaginary parts of the bispectrum) at about 2.5 m depth are shown in figure 10. For both data sets most bispectral energy is concentrated near those frequency pairs with the highest bicoherences. Although for the narrow-band 2 February data relatively few triads are contributing to the bispectrum, while the broad-band data of 15 February are characterized by interactions spread over many frequency pairs within the energetic part of the spectrum, the net band-passed skewness and asymmetry for both data sets are quite similar (figure 9).

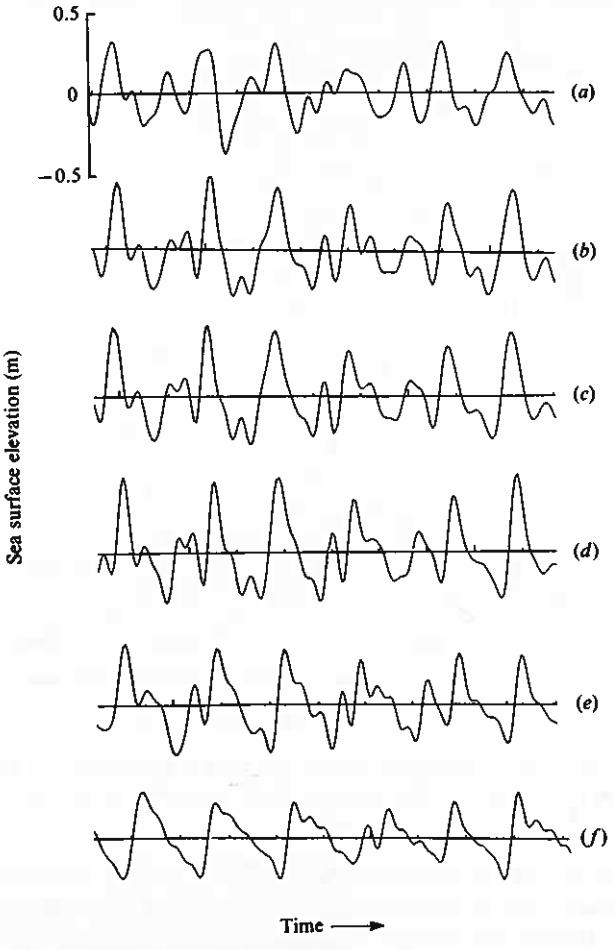

FIGURE 8. Sea-surface elevation *versus* time for a short section (about 90 s) of the 15 February data set. (*a*) $h = 8.4$ m, (*b*) 3.2 m, (*c*) 2.5 m, (*d*) 1.9 m, (*e*) 1.3 m, (*f*) 0.6 m.

For both data sets (figure 10), the contributions from the frequency pairs with low-frequency components [e.g. $b(0.06, 0.01)$] is opposite in sign to the contributions from the high-frequency pairs, and would reduce the skewness shown in figure 9 by 30–60 %. The asymmetry (figure 9) would be reduced by about 15–30 %. The reduction in magnitude of skewness and asymmetry due to interactions involving very low frequencies is consistent with the observed values of biphase (discussed in §4.2), $\pi > \beta > \frac{1}{2}\pi$. Biphases in this quadrant have bispectra with negative real and positive imaginary parts.

The bispectral calculations for the narrow-band 2 February data are consistent with the nonlinear transfer of energy from the power-spectral-peak frequency to higher frequencies via (quadratic) sum interactions. On the other hand, the 12 February data (figure 11, significant wave height in 4 m depth is 56 cm) have double-peaked power spectra with a narrow-swell peak at $f = 0.07$ Hz and a broad sea peak above $f = 0.24$ Hz, and suggest that excitation of modes through difference interactions can also be important. The bicoherence spectra for 12 February (figure 11) are consistent with nonlinear coupling within the lower-frequency swell peak ($b(0.07, 0.07) = 0.24$ at 2.1 m depth) transferring energy through sum

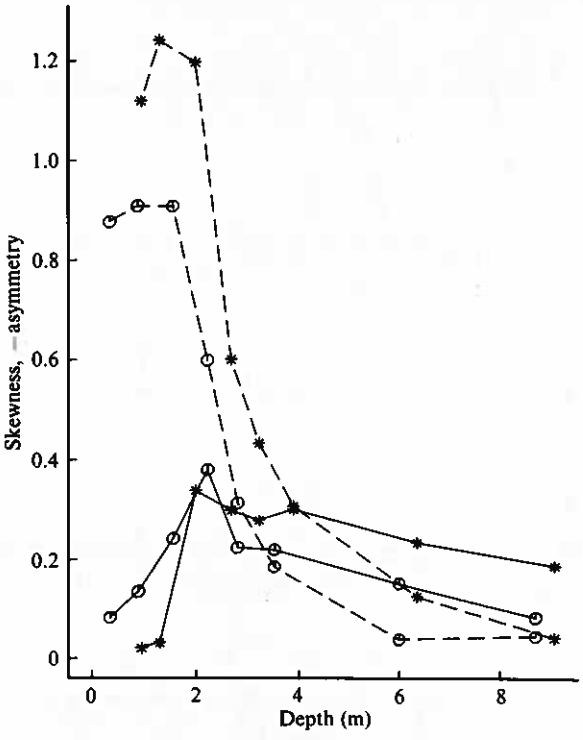

FIGURE 9. Skewness and −asymmetry *versus* depth: ✳ 2 February; ⊙, 15 February; ——, skewness; – – –, −asymmetry. The data are band-pass filtered between 0.04 and 0.4 Hz.

interactions to modes in the spectral valley ($f \sim 0.14$ Hz). Simultaneously, there is coupling between the low-frequency swell peak and the high-frequency sea peak (e.g. $b(0.05, 0.19) = 0.13$ at 2.1 m depth), consistent with a difference interaction between $f = 0.24$ and $f = 0.05$ Hz transferring energy into the spectral valley at $f = 0.19$ Hz. By 1.3 m depth (figure 11*c*) the spectral valley and the high-frequency peak are almost equal in energy, and the sea–swell interactions are weaker than in deeper water ($b(0.05, 0.19) = 0.04$ at 1.3 m depth). The large increase in energy in the spectral valley, and decrease in energy in the sea peak are not predicted by linear theory. Finally, in very shallow water, after some breaking has occurred (0.8 m depth, figure 11*d*), the spectral valley has disappeared, and the energy spectrum is unimodal (above $f = 0.04$ Hz). The biphase spectra of the 12 February data (figure 11) differ from those of the 2 February (figure 3) and 15 February (figure 7) data. As shown in figure 11, in the regions of non-zero bicoherence there are three distinct regimes of biphase. The frequency pairs within the low-frequency swell peak ($f = 0.07$ Hz) undergoing sum interactions have biphases similar to the previously described data sets, with, for example, $\beta(0.07, 0.07)$ evolving from near zero to approximately $-\frac{1}{2}\pi$ as the waves progress from 9 m to 1 m depth (β_1 in figure 11). Sum interactions between sea and swell show similar biphases (β_3 in figure 11). On the other hand, as shown in figure 11 (β_2) and figure 12, the frequency pairs corresponding to difference interactions between sea and swell peaks ((0.05, 0.19), for example) have biphase values that evolve from close to π in deeper water to about 140° just prior to breaking. The biphase values measured in 6 m depth (figure 12) are consistent with the biphase of π for a bound wave produced by a Stokes-like difference interaction. However, similar to the

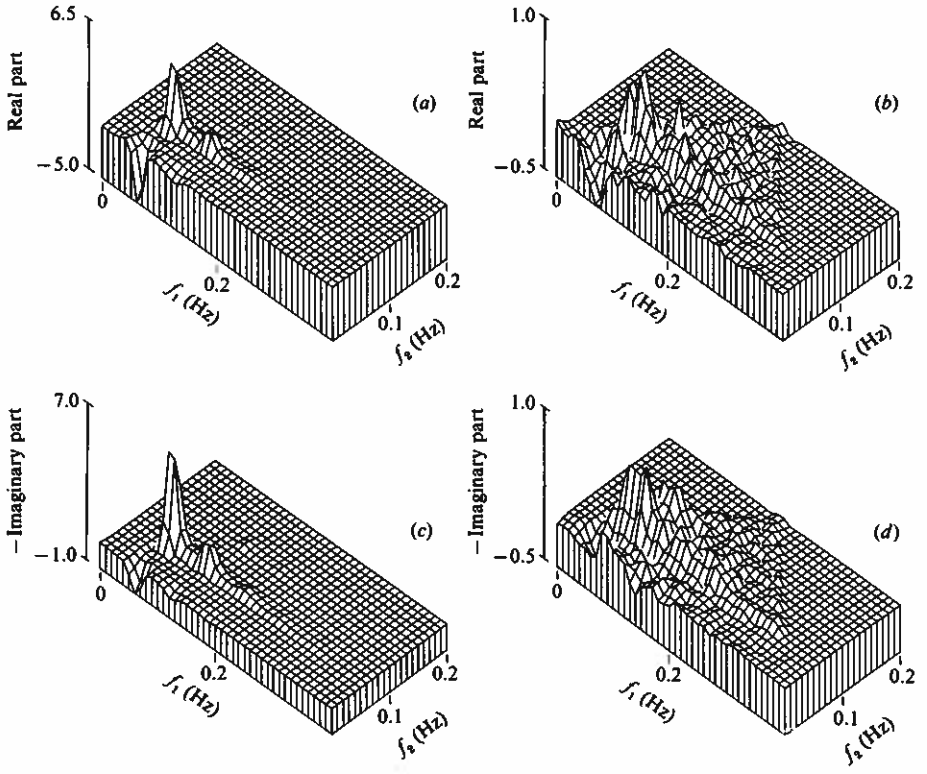

FIGURE 10. Real and −imaginary parts of the bispectrum. The values are normalized such that the volume under the surfaces yields the skewness or asymmetry. The linear vertical scales are arbitrary units, used to show relative scale only. (*a*) Real part 2 February, $h = 2.7$ m; (*b*) real part, 15 February, $h = 2.2$ m; (*c*) −imaginary part, 2 February, $h = 2.7$ m; (*d*) −imaginary part, 15 February, $h = 2.2$ m.

sum interactions, the biphase evolves away from the Stokes value (figure 12). It is interesting to note that the real part of the bispectrum for the sea–swell difference interactions is negative, thus tending to cancel the positive contributions to skewness from the frequency pairs within the swell peak, similar to the effects of very low frequencies ($f < 0.04$) mentioned above. By the shallowest sensor (figure 11*d*), in the zone of wave breaking, the biphases of those frequency pairs previously associated with sea–swell difference interactions have changed substantially, and resemble the biphases of the frequency pairs within the low-frequency swell peak.

4.2. *Infragravity frequencies* ($f < 0.04$ Hz)

The discussion above concentrated on interactions within the swell and wind-wave frequency band of the energy spectrum. However, there is considerable interest in the infragravity wave band ($f < 0.04$ Hz), evident in the shallower-water energy spectra of all the data sets discussed above (figures 2, 6, 11 and also 15). A detailed study of the spatial structure and energy levels of the low-frequency motions observed in this experiment can be found in Guza & Thornton (1985). It has been suggested that energy at infragravity wave frequencies is nonlinearly coupled to the wind-wave frequency band. Specifically, it was shown by Longuet-Higgins & Stewart (1962, 1964) that the beating of two neighbouring high-frequency waves produces a bound, low-frequency long wave that is π out of phase with the envelope of the

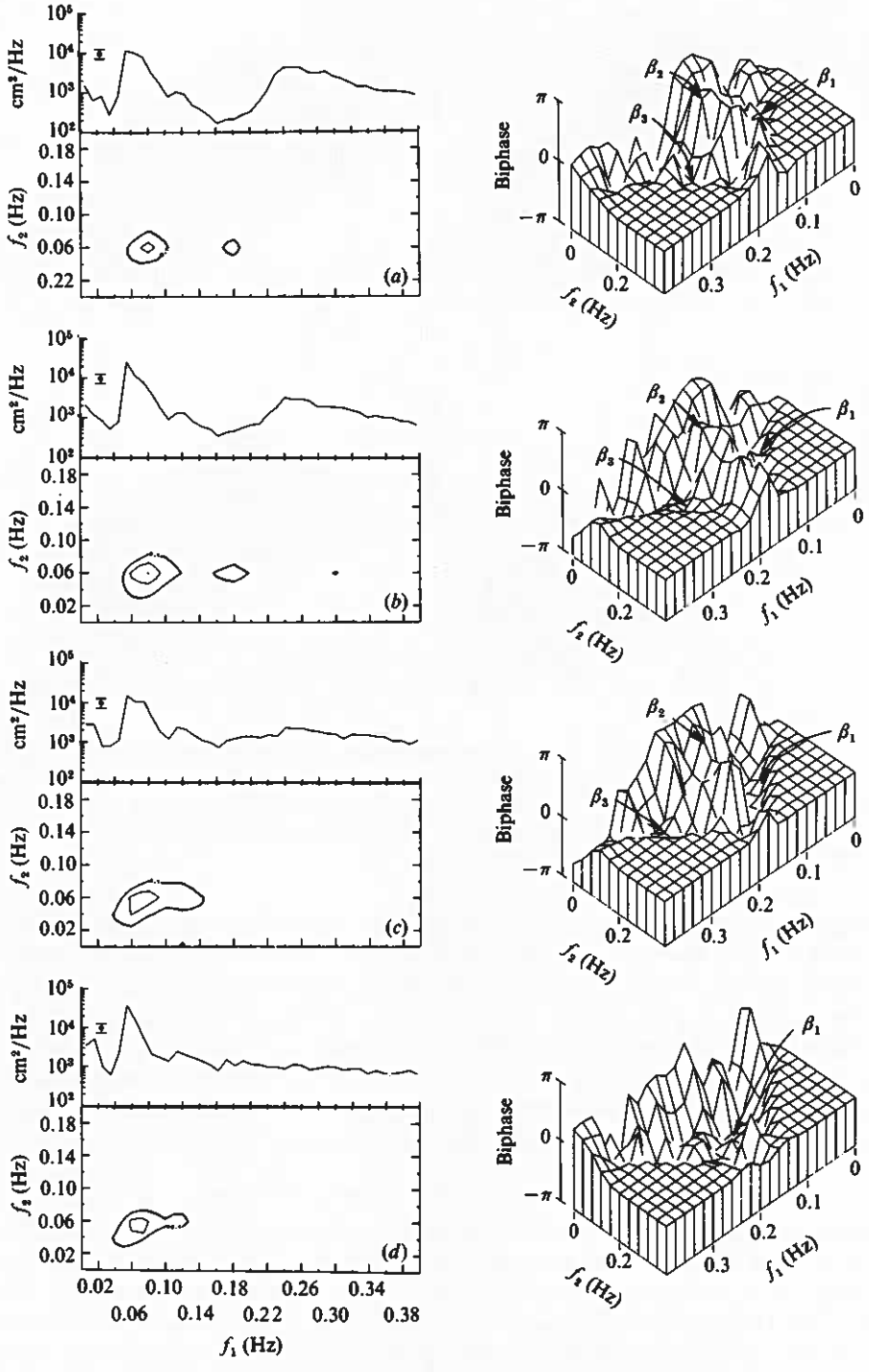

FIGURE 11. Power spectra, contours of bicoherence (with the same format as figure 2), and biphase for the 12 February data set: d.o.f. = 260, and the 95 % significance level ((2.13)) for zero bicoherence is $b = 0.15$. Biphase values are displayed to the right of corresponding bicoherence plots. β_1 indicates swell–swell sum interactions, β_2 sea–swell difference interactions, β_3 swell–sea sum interactions. Depths are (*a*) $h = 3.4$ m, (*b*) 2.1 m, (*c*) 1.4 m, (*d*) 0.8 m.

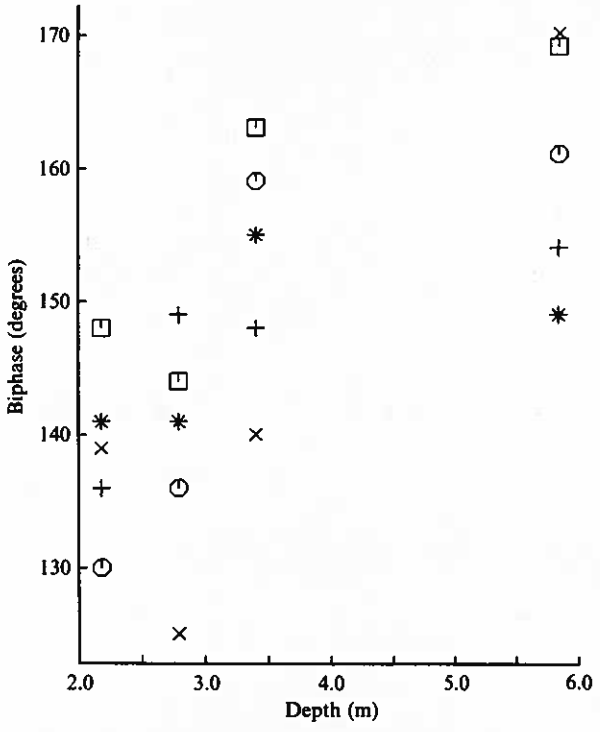

FIGURE 12. Biphase *versus* depth for selected frequency pairs for the 12 February data set: × (0.05, 0.17); ⏲ (0.05, 0.19); ⊡ (0.05, 0.21); + (0.07, 0.17); ✳ (0.07, 0.19).

high-frequency waves. The biphase of the wave triad with frequencies ω_n, ω_m, and $\omega_{n-m} = \omega_n - \omega_m$ is $\beta(\omega_{n-m}, \omega_m) = \pi$.

In a field experiment with limited (16) degrees of freedom, Suhayda (1972, 1974) did not observe significant bicoherence ($b_{95\%} > 0.6$) values for very shallow-water interactions involving surf beat. There are two primary differences between Suhayda's work and the present results, which do show statistically significant nonlinear coupling. First, there are an order of magnitude more degrees of freedom in the present work, thereby considerably reducing the bicoherence significance levels. The second refinement is the separation of the surf-beat signal into shoreward- and seaward-propagating components. Observations on a wide variety of beaches suggest that surf beat is a standing wave (or at least has a significant seaward-propagating component) in the cross-shore direction (Suhayda 1972, 1974; Guza & Thornton 1985 and references therein). Recall that non-zero bispectral levels require non-random phase relationships between the interacting waves. However, when averaged over a finite-width frequency band, the low-frequency reflected waves will have phase relationships relative to their incoming counterparts that tend to decrease bispectral levels. Indeed, for the approximately 0.01 Hz bandwidth used here, the range of wavelengths within the band $f = 0.01$ to $f = 0.02$ Hz is, very roughly, 440–220 m in 2 m depth, resulting in widely varying phase relationships between incoming and reflected waves across the frequency band. Consequently, removing the reflected waves from the time series should increase the bicoherence of frequency pairs involving low-frequency modes. The colocated pressure-gauge–current-meter pairs (figure 1) were used to decompose crudely the records into incoming and outgoing

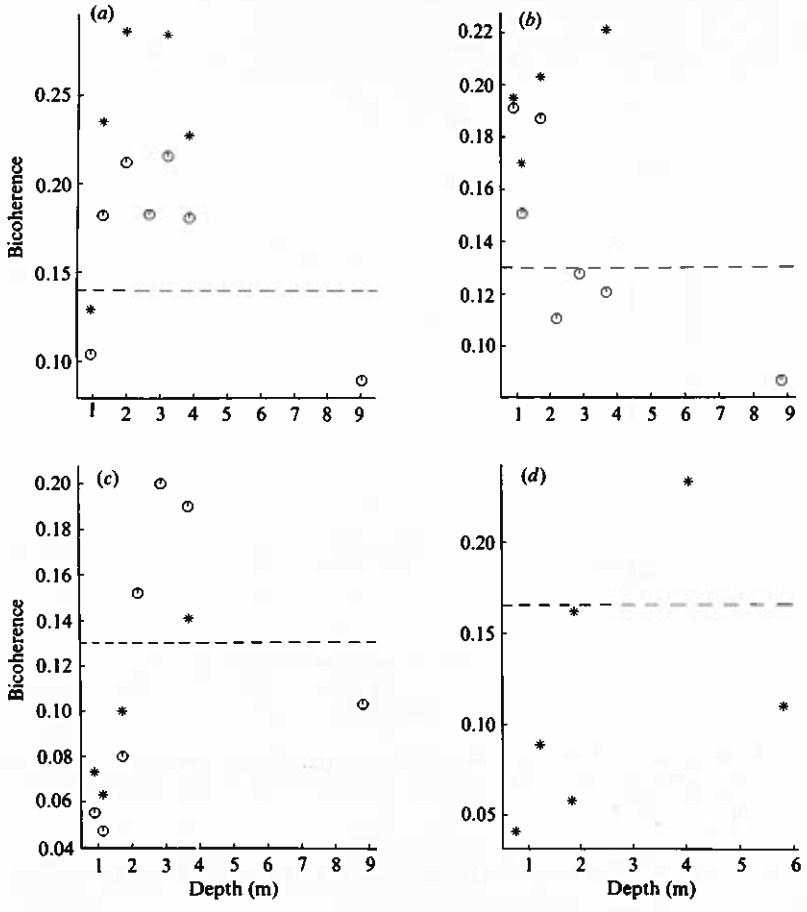

FIGURE 13. Bicoherence *versus* depth for typical frequency pairs which include a low-frequency mode. ⊙, both incoming and reflected low-frequency energy included in the record; ✳ record with reflected energy below $f = 0.04$ Hz removed; ----, 95% significance level ((2.13)) for zero bicoherence. (*a*) 2 February (0.01, 0.06); (*b*) 4 February (0.02, 0.05); (*c*) 4 February (0.02, 0.06); (*d*) 19 November (0.01, 0.06).

waves for $f < 0.04$ Hz (Guza, Thornton & Holman 1984). Bispectral calculations were performed on records with only incoming energy below $f = 0.04$ Hz, but no changes above $f = 0.04$ Hz. Comparisons of bicoherence for frequency pairs (f_Δ, f_p), where f_Δ is a low-frequency ($f_\Delta \approx 0.01$, 0.02 Hz) mode and f_p is the frequency of the power-spectral peak, were made between records with and without reflected surf-beat energy. As expected, removing the long-wave reflections increased the bicoherence levels of almost all the pertinent frequency pairs (figure 13*a–c*), typically by about 25%, but by as much as 100% in some cases. Bicoherences for records with only outgoing energy below $f = 0.04$ Hz (not shown) were substantially lower than all the corresponding values shown in figure 13(*a–c*), and lower than three of the six values shown in figure 13*d*. It is quite clear (figure 13) that statistically significant nonlinear coupling occurs between neighbouring frequencies within the power-spectral peak, and their difference frequency. The 19 November data (figure 13*d*, obtained at Torrey Pines, California; beach slope = 0.02) are included to demonstrate that this type of nonlinear interaction occurs on different beaches.

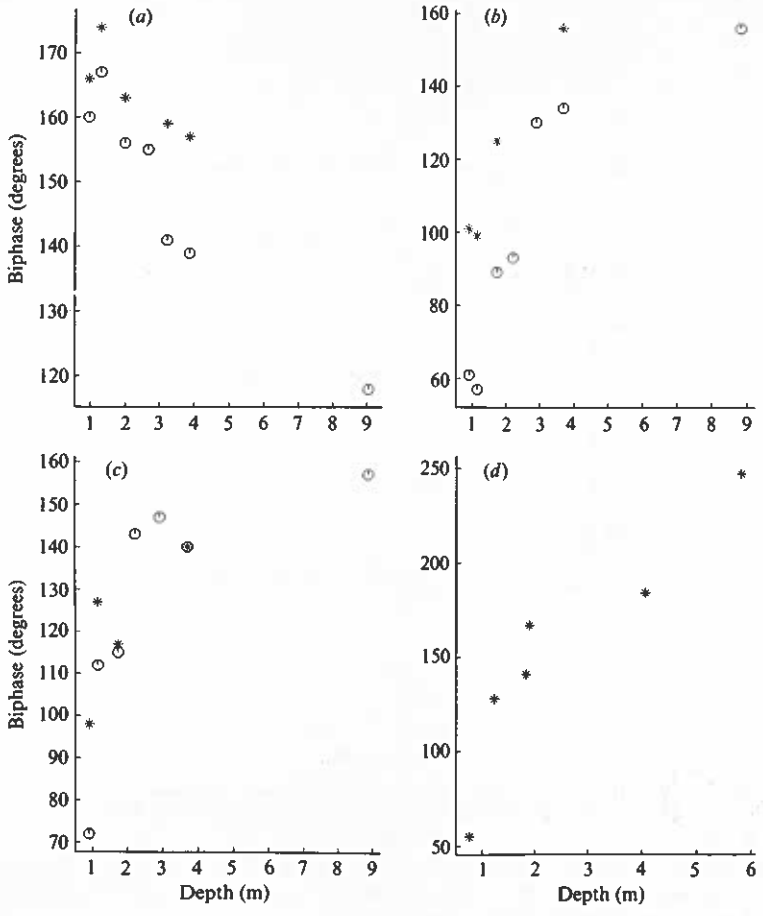

FIGURE 14. Biphase *versus* depth for selected frequency pairs including a low-frequency mode: ⊙, both incoming and reflected energy included in the record: ✳, record with reflected energy below $f = 0.04$ Hz removed. (*a*) 2 February (0.01, 0.06); (*b*) 4 February (0.02, 0.05); (*c*) 4 February (0.01, 0.06); (*d*) 19 November (0.01, 0.06).

In a Stokes-type expansion (Longuet-Higgins & Stewart 1962, 1964) the biphase of these surf-beat-type interactions is $\beta = \pi$. As shown in figure 14, at the deepest sensor locations where reflections could be removed, the observed biphase is somewhat different than 180°. It is important to note that $\beta = 180°$ is a deep-water result, and the deepest stations used here for 2 February and 4 February are in only 4 m depth. Similar calculations for data obtained in 18 m depth in a different experiment produced biphases of about $\beta = 170°$ (for frequency pairs comparable to those in figure 14). In most of the cases investigated, the surf-beat biphase evolves toward lower values as the wave field shoals (figure 14). This evolution of surf-beat biphase observed in the field data is not predicted by the classic bound-long-wave model of Longuet-Higgins & Stewart (1962, 1964). The possibility of a breakdown of bound-wave theory because of shallow-water resonances was mentioned by those authors.

4.3. *Cross-bispectra*

As shown above (figure 13), at any particular location in the shoaling region, surf-beat-frequency energy is nonlinearly coupled to high-frequency modes located

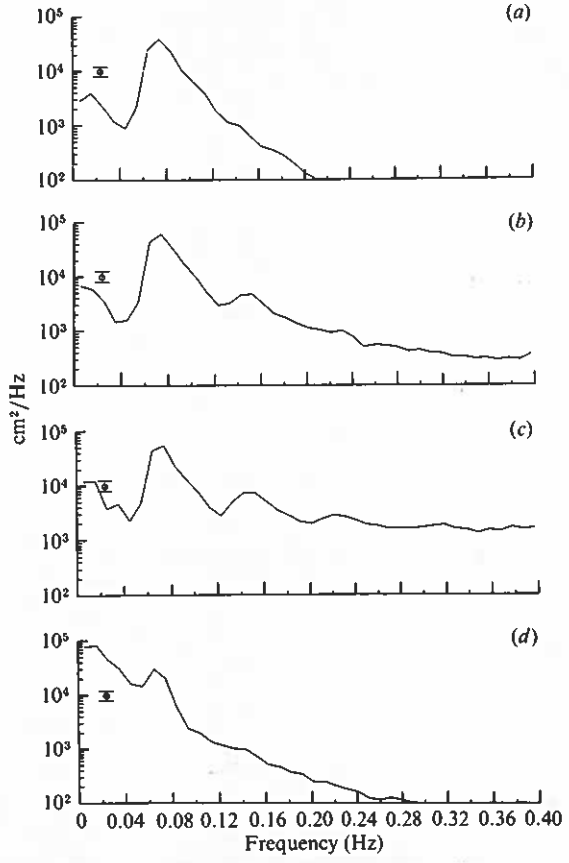

FIGURE 15. Power spectra for 4 February. The bars indicate 95% confidence limits (d.o.f. = 350), and the significant wave height in 3.7 m depth is 88 cm. (*a*) $h = 8.8$ m, (*b*) 3.7 m, (*c*) 1.7 m, (*d*) 0 m. (The data at $h = 0$ were obtained with a runup meter.)

within the power-spectral peak. In the breaking region, high-frequency energy ($f > 0.04$ Hz) is greatly reduced, while lower-frequency energy is increased, relative to their respective levels seaward of the surf zone. This is shown for data obtained 4 February in figure 15 (see also figures 6 and 11). The shallowest sensor, figure 15*d*, is a runup meter and measures swash upon the beach face. It is of interest to know whether or not these very low-frequency surf-beat swash motions are coupled to high-frequency modes in deeper water. In order to investigate this question, cross-bispectra were calculated. The cross-bispectrum is defined here (similar to the auto-bispectrum (2.4)) as

$$XB(f_1,f_2) = \mathrm{E}[A_2(f_1)\,A_1(f_2)\,A_1^*(f_1+f_2)], \tag{4.4}$$

where the A_1 are complex Fourier coefficients measured at one location and the A_2 are Fourier coefficients simultaneously measured at a different location. Other definitions of the cross-bispectrum may be obtained with different combinations of Fourier coefficients. For the present purposes, cross-bispectra for only a few frequency pairs will be considered. Specifically, the A_1 [(4.4)] are Fourier coefficients near the power-spectral-peak frequency, while the A_2 (observed in shallower water than the A_1) represent the small difference of the A_1 frequencies. As shown in figure 16, energy at neighbouring frequencies within the spectral peak measured seaward of the surf

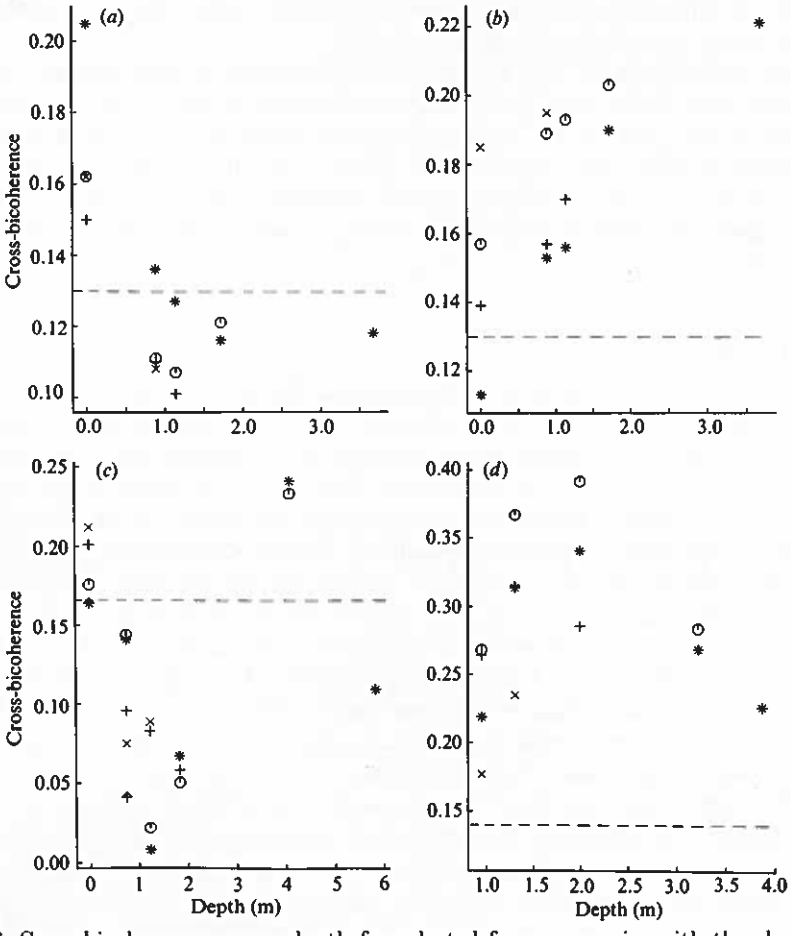

FIGURE 16. Cross bicoherence *versus* depth for selected frequency pairs with the shallower data providing the incoming low-frequency mode (see text). The dashed line is the 95 % significance level ((2.13)) for zero bicoherence. Each symbol represents the cross-bicoherence between a particular depth and all the other depths, as well as the auto-bicoherence at that depth. For example, the asterisks in panel (*a*) represent (from deep to shallow water) the auto-bicoherence observed in 3.7 m depth, cross-bicoherence between $h = 3.7$ and 1.7 m, cross-bicoherence between $h = 3.7$ and 1.1 m, and so on. Each symbol's deep-water depth is: (*a*) 4 February (0.01, 0.06); ✳, 3.7 m; ⊙, 1.7 m; +, 1.1 m; ×, 0.9 m; (*b*) 4 February (0.02, 0.05); ✳, 3.7 m; ⊙, 1.7 m; +, 1.1 m; ×, 0.9 m; (*c*) 19 November (0.01, 0.06); ✳, 5.8 m, ⊙, 4.1 m, +, 1.8 m; ×, 1.2 m; ⊕, 0.8 m; (*d*) 2 February (0.01, 0.05); ✳, 3.9 m; ⊙, 3.2 m; +, 2.0 m; ×, 1.3 m.

zone is nonlinearly coupled to low-frequency (the difference between the two high-frequency modes) motions within the surf zone. In some cases, the cross-bicoherence increases substantially as the depth of the shallow sensor used in the calculations decreases (figure 16*a*; figure 16*c* shoreward of 4 m depth). Indeed, in these two cases (shoreward of 4 m depth) the cross-bicoherence between deeper locations and the runup meter is higher than the auto-bicoherences (at the same frequencies) of the deeper sensors. On the other hand, the opposite trend is observed for the same data set as that shown in figure 16*a*, but for a slightly different set of frequencies, with a higher difference frequency, figure 16*b*. In this case, as the shallower sensor of the pair decreases in depth, the bicoherence also decreases. Note

that for the 2 February data (figure 16*d*) no runup meter was available, and the shallowest sensor is in about 1 m depth.

It is clear from figure 16 that low-frequency motions in very shallow water, and on the beach face itself, are significantly nonlinearly coupled to higher-frequency modes (within the peak of the power spectrum) seaward of the surf zone. At the present time not much more can be said. There is no obvious trend in the values of cross-bicoherence as the shallower sensor decreases in depth (figure 16). Finer frequency resolution than is available with the present data (about 0.01 Hz) would be very useful.

5. Conclusions

The nonlinear evolution of shoaling ocean-surface gravity waves is particularly well suited for bispectral analysis. The development of harmonics as a wave field with a narrow-band energy spectrum shoals is clearly due to quadratic interactions between the power-spectral peak and its harmonics (figure 2). The same type of nonlinear interaction occurs among a wide range of frequencies when the shoaling wave field has a broad-band power spectrum (figure 7). Other similarities in the nonlinear evolution of narrow-band and broad-band power spectra are seen in the bispectrum. For example, the biphases of both data sets evolve from mostly random values in 9 m water depths to a value which is constant over most frequency pairs in the wind-wave band ($0.04 < f < 0.4$ Hz), approaching $\beta = -\frac{1}{2}\pi$ as the waves shoal (figures 3, 4 and 7). The biphase values associated with significant bicoherence levels in 9 m depth are consistent with Stokes-like nonlinearities (at least for narrow-band data). However, as the water depth decreases, the waves evolve through a slightly skewed, somewhat asymmetrical (with respect to a vertical axis) shape, toward a highly asymmetrical, unskewed, sawtooth-like shape (figures 5, 8 and 9). The real and imaginary parts of the bispectrum are, respectively, the contributions to skewness and asymmetry from individual frequency pairs (figure 10). It is seen, figure 10 for example, that interactions involving low (surf-beat) frequencies tend to reduce sea-surface-elevation skewness and asymmetry. Bicoherence and biphase calculations provide evidence for excitation of Fourier modes via difference interactions as well as sum interactions for a data set with a double-peaked power spectrum (figure 11). Low-frequency motions (surf beat) are seen to be coupled to high-frequency energy located within the power-spectral peak (figure 13). These infragravity modes do not appear to be bound with a fixed phase relationship to the high-frequency wave groups since their biphases evolve as the wave field shoals (figure 14). Cross-bispectral calculations demonstrate that low-frequency motions on the beach face (swash) are nonlinearly coupled to higher-frequency (within the power-spectral peak) energy seaward of the surf zone (figure 16). Thus locally forced motions, as well as free (or nearly free) edge waves, contributed to the observed surf-beat-elevation field. A weakly nonlinear model (Freilich & Guza 1984) based on the Boussinesq equations for a sloping bottom (Peregrine 1967) accurately predicts the observed structural evolution of bicoherence and biphase (Elgar & Guza 1985*b*). Since the nonlinear model assumes unidirectional, normally incident waves, the correspondence of observations and model results suggests that refractive narrowing of directional spectra does not contribute significantly to the increase in observed bicoherence as the wave field shoals. Although the nonlinear equations support solutions which are waves of nearly permanent form, the observed evolution of biphase is clearly inconsistent with waves of permanent form. Cnoidal wave solutions to the equations require specific initial

conditions (i.e. initial amplitudes and phases). These stringent requirements are not, in general, met in the present experiments, where power spectra are relatively broad-banded, and Fourier phases in 9 m water depth are not generally significantly different than randomly distributed. Numerical modelling of waves propagating over a shallow *flat* bottom indicates that the gross features of power-spectral (Freilich & Guza 1984) and bispectral evolution (Elgar & Guza 1985*b*) are not primarily due to the sloping bottom, but are a direct consequence of the nonlinear interactions.

Support was provided by a grant from the Foundation for Ocean Research (Steve Elgar) and by the Office of Naval Research, Coastal Sciences Branch, under contract number N0014-75-C-0300 (R. T. Guza). The data collection was supported by ONR and the Sea Grant Nearshore Sediment Transport Study (project number RICA-N-40). Dr E. B. Thornton played a central role in all phases of the experiments. R. L. Lowe was the principal engineer. Dr R. J. Seymour is thanked for encouragement, support, and helpful discussions during the course of this study.

REFERENCES

Barnett, T. P., Johnson, L. C., Naitoh, P., Hicks, N. & Nute, C. 1971 Bispectrum analysis of electroencephalogram signals during waking and sleeping. *Science* **172**, 401–402.

Brillinger, D. R. 1965 An introduction to polyspectra. *Ann. Math. Statist.* **36**, 1351–1374.

Brillinger, D. R. & Rosenblatt, M. 1967*a* Asymptotic theory of estimates of k-th order spectra. In *Advanced Seminar on Spectral Analysis of Time Series* (ed. B. Harris), pp. 153–188. Wiley.

Brillinger, D. R. & Rosenblatt, M. 1967*b* Computation and interpretation of k-th order spectra. In *Advanced Seminar on Spectral Analysis of Time Series* (ed. B. Harris), pp. 189–232. Wiley.

Elgar, S. & Guza, R. T. 1985*a* Shoaling gravity waves: comparisons between field observations, linear theory, and a nonlinear model. *J. Fluid Mech.* **158**, 47–70.

Elgar, S. & Guza, R. T. 1985*b* Nonlinear model predictions of shallow water gravity wave bispectra. Submitted to *J. Fluid Mech.*

Elgar, S., Guza, R. T. & Seymour, R. J. 1984 Groups of waves in shallow water. *J. Geophys. Res.* **89**, 3623–3634.

Freilich, M. H. & Guza, R. T. Nonlinear effects on shoaling surface gravity waves. *Phil. Trans. R. Soc. Lond.* A **311**, 1–41.

Gable, C. G. (ed.) 1981 Report on data from the Nearshore Sediment Transport Study experiment at Leadbetter Beach, Santa Barbara, California, January–February, 1980. *IMR Ref. 80–5.*, University of California., Inst. of Marine Resources, La Jolla, CA.

Godfrey, M. D. 1965 An exploratory study of the bispectrum of economic time series. *Appl. Statist.* **14**, 48–69.

Guza, R. T. & Thornton, E. B. 1985 Observations of surf beat. *J. Geophys. Res.* **90**, 3161–3172.

Guza, R. T., Thornton, E. B. & Holman, R. A. 1984 Swash on steep and shallow beaches. In *Proc. 19th Coastal Enging Conf.*, pp. 708–723. Houston, Texas, American Society of Civil Engineers.

Hasselman, K., Munk, W. & MacDonald, G. 1963 Bispectra of ocean waves. In *Time Series Analysis* (ed. M. Rosenblatt), pp. 125–139. Wiley.

Haubrich, R. A. 1965 Earth noises, 5 to 500 millicycles per second, 1. *J. Geophys. Res.* **70**, 1415–1427.

Helland, K. N., Van Atta, C. W. & Stegun, G. N. 1977 Spectral energy transfer in high Reynolds number turbulence. *J. Fluid Mech.* **79**, 337–359.

Hinich, M. J. & Clay, C. S. 1968 The application of the discrete Fourier transform in the estimation of power spectra, coherence, and bispectra of geophysical data. *Rev. Geophys.* **6**, 347–363.

HUBER, P. J., KLEINER, B., GASSER, T. & DUMERMATH, G. 1971 Statistical methods for investigating phase relations in stationary stochastic processes. *IEEE Trans. Audio and Electroacoustics* **19**, 78–86.

JENKINS, G. M. & WATTS, D. G. 1968 *Spectral Analysis and its Applications*. Holden-Day.

KIM, Y. C., BEALL, J. M., POWERS, E. J. & MIKSAD, R. W. 1980 Bispectrum and nonlinear wave coupling. *Phys. Fluids* **23**, 250–263.

KIM, Y. C. & POWERS, E. J. 1978 Digital bispectral analysis of self-excited fluctuation spectra. *Phys. Fluids* **21**, 1452–1453.

KIM, Y. C. & POWERS, E. J. 1979 Digital bispectral analysis and its application to nonlinear wave interactions. *IEEE Trans. Plasma Science* **1**, 120–131.

LII, K. S., ROSENBLATT, M. & VAN ATTA, C. 1976 Bispectral measurements in turbulence. *J. Fluid Mech.* **77**, 45–62.

LONGUET-HIGGINS, M. S. & STEWART, R. W. 1962 Radiation stress and mass transport in gravity waves, with application to 'surf beats'. *J. Fluid Mech.* **13**, 481–504.

LONGUET-HIGGINS, M. S. & STEWART, R. W. 1964 Radiation stresses in water waves; a physical discussion with applications. *Deep-Sea Res.* **11**, 529–562.

MASUDA, A. & KUO, Y. Y. 1981 A note on the imaginary part of bispectra. *Deep-Sea Res.* **28**, 213–222.

MCCOMAS, C. H. & BRISCOE, M. G. 1980 Bispectra of internal waves. *J. Fluid Mech.* **97**, 205–213.

MUNK, W. H. 1949 Surf beats. *Trans. Am. Geophys. Un.* **30**, 849–854.

PEREGRINE, D. H. 1967 Long waves on a beach. *J. Fluid Mech*, **27**, 815–827.

ROSENBLATT, M. & VAN NESS, J. W. 1965 Estimation of the bispectrum. *Ann. Math. Statist.* **36**, 1120–1136.

SATO, T., SASAKI, K. & TAKETANI, M. 1980 Bispectral passive velocimeter of a moving noisy machine. *J. Accoust. Soc. Am.* **68**, 1729–1735.

SUHAYDA, J. N. 1972 Experimental study of the shoaling transformation of waves on a sloping bottom. Ph.D. dissertation, Scripps Institution of Oceanography, University of California, La Jolla, CA.

SUHAYDA, J. N. 1974 Standing waves on beaches. *J. Geophys. Res.* **72**, 3065–3071.

VAN ATTA, C. W. 1979 Inertial range bispectra in turbulence. *Phys. Fluids* **22**, 1440–1443.

YEH, T. T. & VAN ATTA, C. W. 1973 Spectral transfer of scales and velocity fields in heated-grid turbulence. *J. Fluid Mech.* **58**, 233–261.